Inorganic Chemistry

Article

pubs.acs.org/IC

Photoluminescence Properties of Eu^{3+}-Doped Glaserite-Type Orthovanadates $CsK_2Gd[VO_4]_2$

Zhengxu Tao,[†] Taiju Tsuboi,[‡] Yanlin Huang,[†] Wei Huang,[‡] Peiqing Cai,[§] and Hyo Jin Seo*[,§]

[†]College of Chemistry, Chemical Engineering, and Materials Science, Soochow University, Suzhou 215123, China

[‡]Institute of Advanced Material, Nanjing Tech University, Nanjing 210009, China

[§]Department of Physics and Center for Marine-Integrated Biomedical Technology, Pukyong National University, Busan 608-737, Republic of Korea

ABSTRACT: Undoped and Eu^{3+}-doped glaserite-type orthovanadates $CsK_2Gd_{1-x}Eu_x[VO_4]_2$ with various Eu^{3+} concentrations of x = 0, 0.1, 0.2, 0.3, 0.4, 0.5, 0.6, 0.7, 0.8, 0.9, and 1.0 were synthesized via the solid-state reaction. The formation of a single phase compound was verified through the X-ray diffraction studies. The photoluminescence (PL) and PL excitation (PLE) spectra, PL decay curves, and absolute quantum efficiency (QE) were investigated. Unlike the conventional Eu^{3+}-doped vanadates, these Eu^{3+}-doped samples showed not only several sharp emission lines due to Eu^{3+} but also a broad emission band with a maximum at 530 nm due to the $[VO_4]^{3-}$ host. The intensities of the host and Eu^{3+} emissions increased when the Eu^{3+} concentration was increased from x = 0 to x = 0.6 and decreased above x = 0.6. Similar concentration dependence was observed for QE. The host emission, even if in the Eu^{3+}-condensed host of $CsK_2Eu(VO_4)$, was never quenched indicating inefficient energy transfer from the host $[VO_4]^{3-}$ to Eu^{3+}. This inefficient energy transfer is understood by suppression of the energy transfer by the V—O—Eu bond angle deviated from 180° and the separation of Eu^{3+} ions at the Gd^{3+} site from $[VO_4]^{3-}$. Like the 530 nm charge transfer $[VO_4]^{3-}$ emission, two broad and intense PLE bands with maxima at 330 and 312 nm were observed for the Eu^{3+} emission. A maximum QE of 38.5% was obtained from $CsK_2Gd_{1-x}Eu_x[VO_4]_2$ (x = 0.6). A white-colored emission was obtained by the combination of the broad 530 nm emission band and the intense sharp lines due to Eu^{3+} at 590−620 nm.

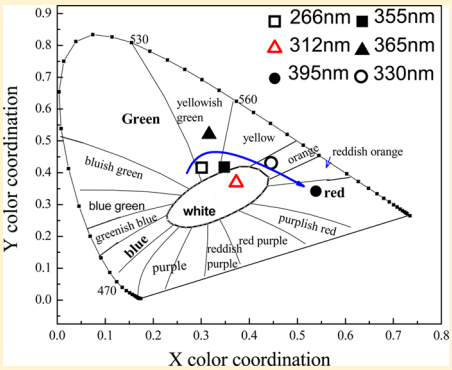

1. INTRODUCTION

Undoped and rare-earth (RE) ion-doped vanadates are known as luminescence materials with rich colors, high luminescence efficiencies, and excellent chemical stabilities.[1−6] $[VO_4]^{3-}$ in vanadate crystals gives rise to intense charge transfer (CT) absorption bands in the near-ultraviolet (UV) region and a broad emission band at 400−700 nm.[1] Therefore, the vanadates are expected to be phosphors for white light emitting diodes (W-LEDs) which are used in lighting and flat-panel displays (FPDs).[7,8]

Of various RE-doped vanadates, Eu^{3+}-doped orthovanadates have been intensively investigated because of their high efficiency, long lifetimes, and environment-friendly characteristics.[9−11] For example, Eu^{3+}-doped orthovanadates RVO_4:Eu^{3+} (R = La, Gd, Y, Lu) are excellent phosphors with bright red emission.[12−14] Especially YVO_4:Eu^{3+} is a commercially available red phosphor for high pressure Hg-lamps, which can efficiently convert 314−365 nm photons into red light and maintain highly efficient luminescence at high temperatures.[15] Eu^{3+}-doped vanadate−garnets such as $Ca_2NaMg_2V_3O_{12}$:Eu^{3+},[9] $EuNa_2Mg_2(VO_4)_3$,[16] and $Bi_xLn_yEu_{1-x-y}Na_2Mg_2V_3O_{12}$ (Ln = Y, La, Gd; x = 0−0.4; and y = 0−0.2)[3] have been considered to be red phosphors for W-LEDs.

The present work was undertaken to find a new vanadate host for Eu^{3+} ions. Here we chose $CsK_2Gd[VO_4]_2$ because, to the best of our knowledge, the luminescence properties of neither undoped nor doped $CsK_2Gd[VO_4]_2$ have been reported. $CsK_2Gd[VO_4]_2$ belongs to a family of orthovanadates with glaserite-like structure. The prototype of this compound is the sulfate $K_3Na(SO_4)_2$. It is described by the formula $XY_2M(TO_4)_2$ where X, Y, M, and T are cationic sites of 12, 10, 6, and 4 coordination, respectively. Glaserite-like orthovanadates have been gaining attention because of applications to luminescence materials, for example, $K_3Y(VO_4)_2$ doped with Dy and $K_3Y(VO_4)_2$ codoped with Dy and Bi,[17] $A_3RE(VO_4)_2$ (A = alkali metal, RE = Sc, Y, La−Lu),[18] and $Na_3Ln(VO_4)_2$ (Ln = La, Nd, and Er).[19]

Optical properties have been studied for various Eu^{3+}-doped vanadates; however, most studies have been for the emission due to Eu^{3+} ions. No detailed study has been made for the cases of the coexistence of emissions due to the host $[VO_4]^{3-}$ and the dopant Eu^{3+}. We are trying to find not only emission from Eu^{3+} but also emission from the host in $CsK_2Gd[VO_4]_2$, and then we will discuss the reason for coexistence. The doping of metal ions like RE ions in vanadate has been expected to increase the photoluminescence (PL) intensity and quantum efficiency (QE).[8] This, however, has not been confirmed experimentally

Received: January 27, 2014
Published: April 7, 2014

   dx.doi.org/10.1021/ic500208h | Inorg. Chem. 2014, 53, 4161−4168

for Eu^{3+}-doped vanadates. Here we study the PL spectra and PL quantum efficiencies of $CsK_2Gd_{1-x}Eu_x[VO_4]_2$ with various Eu^{3+} concentrations of x = 0, 0.1, 0.2, 0.3, 0.4, 0.5, 0.6, 0.7, 0.8, 0.9, and 1.0, together with the PL excitation (PLE) spectra and the decay curves, to clarify the influence of Eu^{3+}.

2. EXPERIMENTAL SECTION

The polycrystalline $CsK_2Gd_{1-x}Eu_x[VO_4]_2$ (x = 0−1.0) was synthesized via the solid-state reaction. The starting material was a stoichiometric mixture of reagent grade NH_4VO_3, Cs_2CO_3, K_2CO_3, and RE_2O_3 (RE = Gd, Eu). First, the stoichiometric mixture was slowly heated up to 350 °C in 7 h and was kept at this temperature for 5 h. The obtained powder was mixed again and then heated up to 700 °C for 5 h in air. The sample was then thoroughly mixed and heated at 780−800 °C for 10 h in air.

The phase purity was checked by powder X-ray diffraction (XRD) analysis collected on a Rigaku D/Max diffractometer (40 kV, 30 mA) and with Bragg−Brentano geometry using Cu Kα radiation (λ = 1.5405 Å). The PL and PLE spectra were recorded on a PerkinElmer LS-50B luminescence spectrometer. For the measurements of luminescence decay curves, the samples were excited by a pulsed Nd:YAG laser at 355 nm (Spectron Laser System SL802G). The luminescence was dispersed by the 75 cm monochromator (ActonResearch Corp. Pro-750) and was multiplied by the photomultiplier (PMT) (Hamamatsu-Photonics Co. R928). The data was displayed and recorded with the LeCloy 9301 digital storage oscilloscope. The absolute QE, that is, the internal QE, was measured by an Absolute Photoluminescence Quantum Yield Measurement System (C9920−03, Hamamatsu-Photonics) at room temperature. This system employs the PL method for measuring the internal QE, which is defined as the ratio of the number of emitted photons to the number of photons absorbed by the material. The excitation wavelength is selected from the output of the xenon lamp by a monochromator. The excitation xenon lamp source, integrating sphere, an ultrahigh sensitivity multichannel charge coupled device (CCD) sensor spectrometer, and a computer with PL measurement software were connected by light guides. The QE value was calculated by quantum yield measurement software.

3. RESULTS AND DISCUSSION

3.1. Crystal Phase Formation and Morphology. The XRD patterns of $CsK_2Gd_{1-x}Eu_x[VO_4]_2$ (x = 0−1.0) are shown in Figure 1a. All patterns are in agreement with the powder diffraction file 2 (PDF2) card No. 54-0946 ($CsK_2Gd[VO_4]_2$) in the International Center for Diffraction Data (ICDD) database. The XRD peaks are well indexed to the hexagonal glaserite-like structure with space group of $P\bar{3}ml$ (No. 164). The crystal structure is never changed by Eu^{3+}-doping even if all Gd^{3+} ions are substituted by Eu^{3+} ions. No signal due to impurity was observed. The cell parameters estimated by a Jade-5.0 software program are shown in Figure 1b. It is obvious that the crystal structure parameters become larger in the sequence of x = 0−1.0. This expansion is due to a larger Eu^{3+} ion radius (0.947 pm in 6-coordinate) than the Gd^{3+} ion radius (0.938 pm in 6-coordinate).

Figure 2a is a sketch map of the $CsK_2Gd[VO_4]_2$ crystal structure on the (110) direction, which was modeled using the Diamond Crystal and Molecular Structure Visualization software based on the atomic coordinate data reported by Melnikov et al.[20] Figure 2b is the schematic portion showing the alignments of Gd(Eu)—O—V in the Eu^{3+}-doped samples. The structure of $CsK_2Gd[VO_4]_2$ is isostructural with the glaserite type, which crystallizes in the trigonal space group $P\bar{3}ml$ and Z = 1. The trigonal axis is the crystallographic c axis. According to the $XY_2M(TO_4)_2$ general formula of the glaserite family, the X, Y, M, and T sites are totally occupied by Cs^+, K^+,

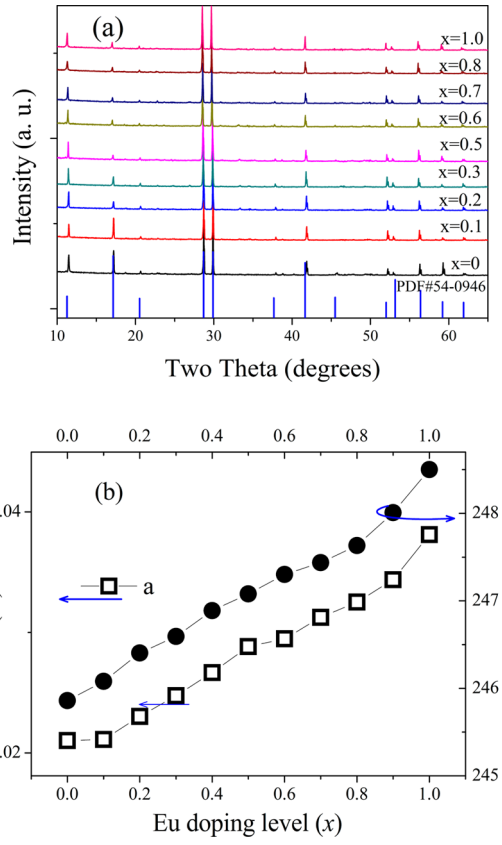

Figure 1. (a) XRD patterns of $CsK_2Gd_{1-x}Eu_x[VO_4]_2$ (x = 0−1.0) orthovanadates and the corresponding PDF2 standard card No. 54−0946; (b) the dependence of the unit cell parameters on the Eu^{3+}-doping.

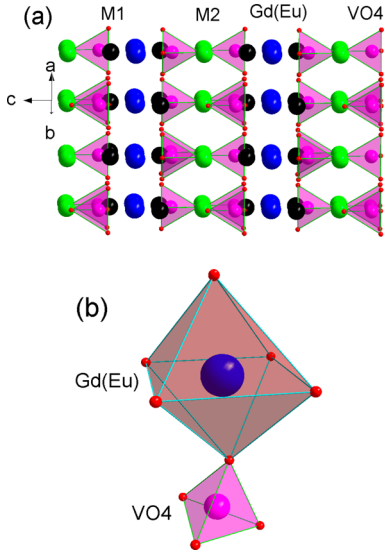

Figure 2. (a) The sketch map of $CsK_2Gd_{1-x}Eu_x[VO_4]_2$ with a glaserite-like structure on the (110) direction. M cation sites are randomly occupied by (K + Cs) shown as black balls for M(1) (0.67 K + 0.33 Cs2) and as green balls for M(2) (0.67 K + 0.33 Cs1); (b) the schematic portion showing the alignments of Eu—O—V in Eu-doped samples. The blue and pink balls are Gd^{3+}(Eu) and V^{5+} ions, respectively.

Gd^{3+}, and V^{5+} cations, respectively.[21] The lattice framework is built up by the stacking of two kinds of corner-shared GdO_6

dx.doi.org/10.1021/ic500208h | Inorg. Chem. 2014, 53, 4161−4168

octahedral and VO_4 tetrahedra parallel to the (a, b) plane. In the layer, each GdO_6 octahedron is linked to six VO_4 tetrahedra and each tetrahedron is connected to three octahedral. The Gd^{3+} ions have an inversion center and occupy only one 6-fold coordinated RE site with a high symmetry of D_{3d}.[20] The cavities of the framework are filled by M(1) and M(2) cations, which are in the arrangements as $M(1)O_{10}$ (0.67K + 0.33Cs) and $M(2)O_{12}$ (0.67K + 0.33Cs), respectively. Both M(1) and M(2) sites are on Wyckoff 2d positions and have 3m symmetry in the chains along (010) direction. In the lattices, the metal V^{5+} ions occupying Wyckoff 2d positions occupy the 4-fold Td site in the distorted tetrahedral environment of VO_4^{3-}, with a V—O bond length in the range of 1.5608(2)−1.5877(1) Å. The V^{5+} ion has a closed-shell electronic structure with no d electron. Considering the electronic structure of the VO_4^{3-} ion in T_d symmetry, the electron CT process from the 2p orbital of O^{2-} to the 3d orbital of the V^{5+} ion is involved in the excitation and the luminescence phenomena.

3.2. Luminescence of an Undoped Sample. Figure 3 presents the PL and PLE spectra of undoped $CsK_2Gd(VO_4)_2$.

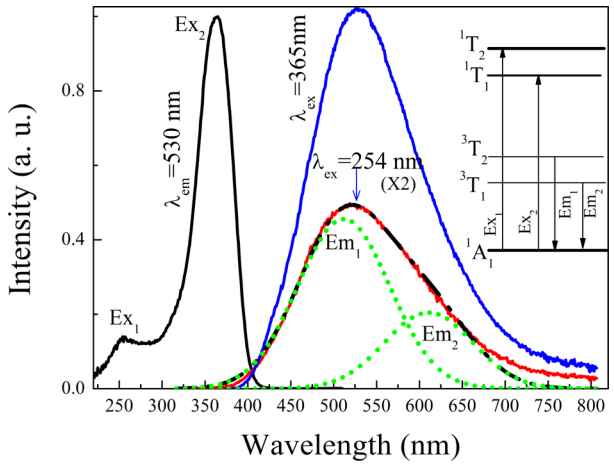

Figure 3. PL and PLE spectra of $CsK_2Gd[VO_4]_2$, the dashed lines are two Gaussian components named as Em_1 and Em_2 by fitting the spectrum. The inset shows the excitation and emission processes in the VO_4 tetrahedron with T_d symmetry.

The sample shows a broad emission band between 400 and 750 nm with a maximum at about 530 nm. The 530 nm emission band is asymmetric, which is decomposed to the two bands Em_1 and Em_2. The origin of this emission has been understood by the CT of an electron from the oxygen 2p orbital to the vacant 3d orbital of V^{5+} in the tetrahedral VO_4.[1,22] VO_4 has the ground state $^1A_1$ and the excited states $^1T_1$, $^1T_2$, $^3T_1$, and $^3T_2$ (inset Figure 3). The absorption-process transitions ($^1T_1$,$^1T_2$ ← $^1A_1$) are allowed, but the luminescence-process transitions ($^3T_1$,$^3T_2$ → $^1A_1$) are forbidden in the ideal T_d symmetry by the spin selection rule. The spin-forbidden transition, however, is partially allowed by the spin−orbit interaction. Since the spin−orbit interaction depends on not only the spin and orbital angular momentums but also the central-field potential,[23] the distortion of VO_4 tetrahedron from the ideal T_d symmetry enhances the spin−orbit interaction.[1,8] Additionally, this transition is also allowed by the spin−orbit interaction because of the heavy atom effect since VO_4 contains the V atom. As a result, an intense 530 nm emission is observed. The PL and PLE spectra of Figure 3 are quite similar to those observed so far in various vanadates. Therefore, like the cases of various vanadates,[1,5,24] the excitation bands Ex_2 and Ex_1 at 365 nm and about 260 nm are attributed to the transitions from the $^1A_1$ state to the $^1T_1$ and $^1T_2$ states, respectively, while the two emission bands Em_1 and Em_2 are attributed to the ($^3T_1$ and $^3T_2$) → $^1A_1$ transitions (see inset Figure 3).

3.3. Luminescence of Eu^{3+}-Activated Samples. Figure 4a shows the PL spectra of Eu^{3+}-doped $CsK_2Gd(VO_4)_2$ (i.e.,

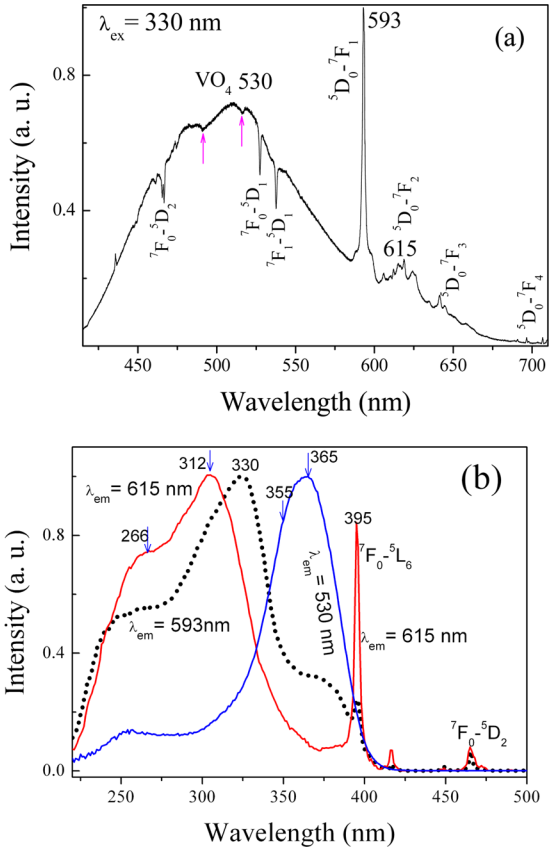

Figure 4. (a) PL spectrum of $CsK_2Gd_{1-x}Eu_x[VO_4]_2$ (x = 0.9) excited at 330 nm. (b) PLE spectra for λ_{em} = 615 nm (from $^5D_0$ → $^7F_2$ of Eu^{3+}), 593 nm ($^5D_0$ → $^7F_1$ of Eu^{3+}), and 530 nm (VO_4).

$CsK_2Gd_{1-x}Eu_x[VO_4]_2$ (x = 0.9)) excited at 330 nm. In addition to the 530 nm broad emission band, which was observed in an undoped $CsK_2Gd(VO_4)_2$ (Figure 3), several sharp emission lines are observed at 580−800 nm. These lines are attributable to the transitions from the excited $^5D_0$ state to the Stark components of the ^7F levels in Eu^{3+}. Five dips are observed in the broad emission band due to $[VO_4]^{3-}$. Of the five dips, three sharp dips at 465, 527, and 537 nm are due to self-absorption by the Eu^{3+} ions, that is, $^5D_2$ ← $^7F_0$ (465 nm), $^5D_1$ ← $^7F_0$ (527 nm), and $^5D_1$ ← $^7F_1$ (537 nm). On the other hand, two broader and weaker dips at 492 and 516 nm (shown by arrows in Figure 4a) are temporarily attributed to another origin such as impurity.

In Eu^{3+}-doped orthovanadates such as YVO_4:Eu^{3+},[14,25] $LaVO_4$:Eu^{3+},[26] $Gd(V_{0.6}P_{0.4})O_4$:Eu^{3+},[26] $Dy:K_3Y(VO_4)_2$,[17] $Dy,Bi:K_3Y(VO_4)_2$,[17] and $Ca_2NaZn_2V_3O_{12}$:Eu^{3+},[28] it is well-known that the host emission from $[VO_4]^{3-}$ is nearly quenched, and the emission lines from Eu^{3+} ions are dominated. This is due to the efficient energy transfer from vanadate $[VO_4]^{3-}$ to RE^{3+} ions. Unlike these Eu^{3+}-doped orthovanadates, our Eu^{3+}-doped $CsK_2Gd(VO_4)_2$ never showed

dx.doi.org/10.1021/ic500208h | Inorg. Chem. 2014, 53, 4161−4168

the quenching of the 530 nm emission even when in heavily Eu^{3+}-doped samples. This indicates that the energy transfer from VO_4^{3-} to Eu^{3+} is inefficient in $CsK_2Gd[VO_4]_2$.

Figure 4b shows the PLE spectra for 530 nm ($[VO_4]^{3-}$), 593 nm ($^5D_0 \rightarrow {}^7F_1$ of Eu^{3+}), and 615 nm ($^5D_0 \rightarrow {}^7F_2$ of Eu^{3+}) emissions. The PLE spectrum for a 530 nm emission consists of two broad bands with maxima at 365 and about 266 nm, which are ascribed to the CT transition in VO_4^{3-} as the case in the undoped sample. On the other hand, the PLE spectra for 593 and 615 nm emissions of Eu^{3+} ions consist of sharp lines at 395 and 465 nm, which are due to the transitions of $^5L_6 \leftarrow {}^7F_0$ and $^5D_2 \leftarrow {}^7F_0$ of Eu^{3+}, respectively, and broad bands in a range of 220−400 nm. The PLE spectrum for a 593 nm emission has broad bands with maxima at 365, 330, 312 (as a small shoulder), and about 266 nm, while the PLE spectrum for a 615 nm emission has bands with maxima at 312 and about 266 nm. From a careful examination of the latter spectrum, it was observed that weak bands are overlapped at about 360 and 330 nm. Therefore, it was found that the two PLE spectra have almost identical bands although the intensity ratio among the four bands is different between the two spectra. Of the four PLE bands, the 365 and 266 nm PLE bands are due to the host because they appear in the undoped sample as mentioned in section 3.2. The appearance of the 365 and 266 nm PLE bands in the PLE spectra for the 593 and 615 nm emissions of Eu^{3+} are understood by the energy transfer from $[VO_4]^{3-}$ to Eu^{3+}. This energy transfer, however, is not efficient because the emission of $[VO_4]^{3-}$ never disappears in the presence of Eu^{3+}. The PLE bands with maxima at 330 and 312 nm have not been observed in undoped $CsK_2Gd[VO_4]_2$ but have been observed in Eu^{3+}-doped $CsK_2Gd[VO_4]_2$. It is noted that the 330 and 312 nm PLE bands were not observed in the previously investigated Eu^{3+}-doped vanadates.[26−28]

Figure 5a shows PL spectra of $CsK_2Gd_{1-x}Eu_x[VO_4]_2$ (x = 0.6) excited at 266, 312, 330, 355, 365, and 395 nm. This phosphor presents different emission profiles under the different excitation wavelengths. Under the excitation at 395 nm, the emission at about 615 nm due to the $^5D_0 \rightarrow {}^7F_2$ transition of Eu^{3+} is much more intense than the emission at 593 nm due to the $^5D_0 \rightarrow {}^7F_1$ transition. The same is observed under excitation at 312 and 266 nm. When excited at 330, 355, and 365 nm, however, the 593 nm emission is much less intense than the 615 nm emission.

The $^5D_0 \rightarrow {}^7F_1$ transition is magnetic-dipole allowed, which leads to a very weak emission intensity. However, a more intense $^5D_0 \rightarrow {}^7F_1$ emission is observed at 593 nm under excitation at 330 nm than the $^5D_0 \rightarrow {}^7F_2$ emission at 615 nm. This suggests that the Eu^{3+} ion has inversion symmetry. The Eu^{3+} and Gd^{3+} ions have very similar ionic radii (0.947 and 0.938 pm for Eu^{3+} and Gd^{3+} in a six-coordinate, respectively); therefore, it is highly conceivable that Eu^{3+} enters the Gd^{3+} sites. The Gd^{3+} site is an inversion center with D_{3d} symmetry.[20] This is consistent with the above-mentioned suggestion that Eu^{3+} demonstrates inversion symmetry.

Taking into account that the 330 and 312 nm PLE bands are not observed in undoped $CsK_2Gd[VO_4]_2$ and that different PL profiles are obtained between the 330 and 312 nm excitations, we suggest that the 330 and 312 nm PLE bands (Figure 4b) are caused by CT from oxygen to Eu^{3+} in the octahedron. The presence of two PLE bands at 330 and 312 nm is understood from the analogy of the CT $[VO_4]^{3-}$ emission which has two PLE bands.

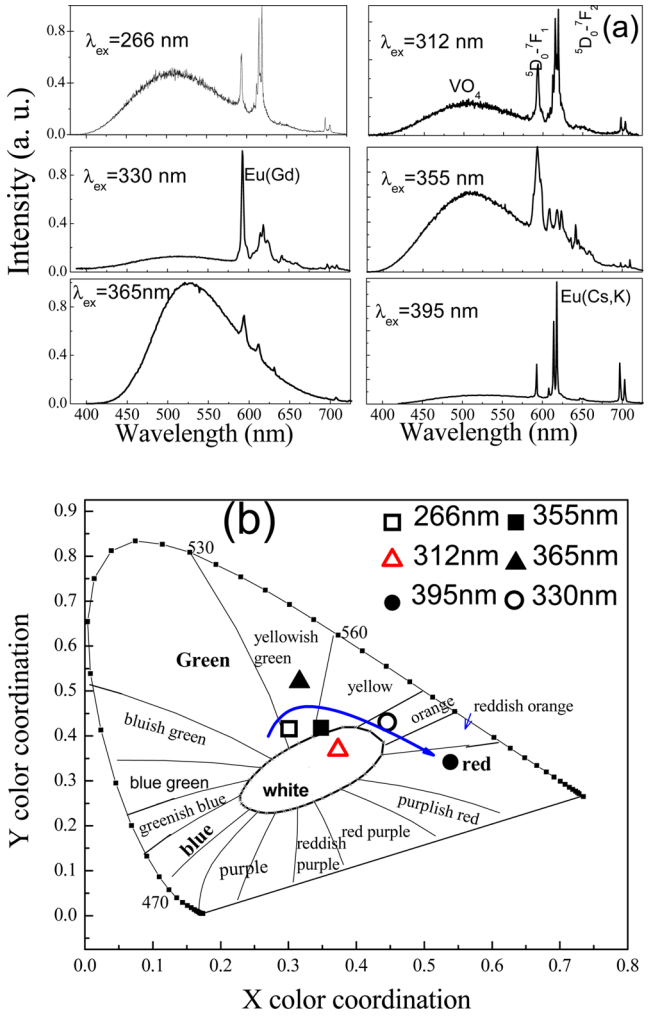

Figure 5. PL spectra (a) and the Commission Internationale de l'Eclairage (CIE) chromaticity coordinates (b) of $CsK_2Gd_{1-x}Eu_x[VO_4]_2$ (x = 0.6) excited at different excitation wavelengths.

$CsK_2Gd_{1-x}Eu_x[VO_4]_2$ gives PL with different colors by changing the excitation wavelength, resulting in rich luminescence colors as displayed by the CIE color coordinates in Figure 5b. It is noted that the excitation of the 312 nm PLE band of Figure 4b leads to white light with CIE coordinates close to CIE (0.33, 0.33) by overlapping with a broad band with a maximum at 530 nm. This indicates that $CsK_2Gd_{1-x}Eu_x[VO_4]_2$ presents tunable emission color and could be useful as a phosphor for UV-LEDs, which are used for lighting.

3.4. The PL Intensity, QEs, and PL Lifetimes. The PL spectra of $CsK_2Gd_{1-x}Eu_x[VO_4]_2$ excited at 312 nm at various Eu^{3+} concentrations are shown in Figure 6a. The intensities of the broad band due to $[VO_4]^{3-}$ and sharp lines due to Eu^{3+} change with an increasing concentration of Eu^{3+}. It was found that both of the emission intensities increased when the concentration increased from x = 0 to x = 0.6, then decreased above x = 0.6. The increase in the VO_4 emission intensity is understood as follows. The ($^3T_1$,$^3T_2 \rightarrow {}^1A_1$) spin-forbidden transitions become allowed by the heavy atom effect because of the nearby Eu^{3+} ions, leading to a high transition rate with the increasing Eu^{3+} concentration. Another reason is that when the Eu^{3+} ion is located near VO_4 it possibly induces distortion of

dx.doi.org/10.1021/ic500208h | Inorg. Chem. 2014, 53, 4161−4168

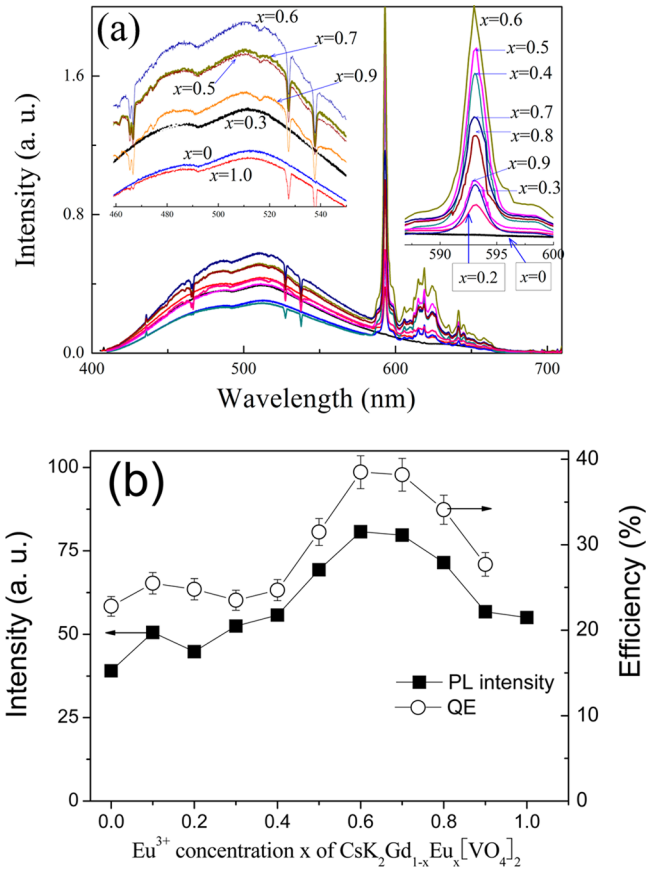

Figure 6. (a) PL spectra of $CsK_2Gd_{1-x}Eu_x[VO_4]_2$ (λ_{ex} = 312 nm). Inset shows the enlargement of the partial spectra. (b) The integrated PL intensity and the PL QE, which are plotted against the Eu^{3+} concentration.

the VO_4 tetrahedron, thus the ($^3T_1$,$^3T_2 \rightarrow {}^1A_1$) spin-forbidden process is partially allowed by the spin−orbit interaction as mentioned in section 3.2, and the distortion is expected to enhance with the increasing Eu^{3+} concentration, leading to an increase in the PL emission intensity.[8]

Since the Eu^{3+} emission lines are superimposed on the 530 nm broad band, it is difficult to estimate the Eu^{3+} emission intensity exactly. Figure 6b displays the plot of the integrated intensity of total emission from the sample against the Eu^{3+} concentration. It is suggested that the decrease in Eu^{3+} emission intensity above x = 0.6 is due to concentration quenching. Two processes are conceivable as the main reasons for the concentration quenching of RE ions such as Eu^{3+} and Pr^{3+}.[29−36] One is a cross-relaxation process which is enhanced at high concentrations; the other is energy migration. The former process occurs between two neighboring Eu^{3+} ions, while the latter process occurs over Eu^{3+} ions in crystal but the migration stops at the quenching sites.

It is curious that the concentration quenching is also observed for the VO_4 emission because of the host, as seen in Figure 6a. This is understood as follows. The energy transfer from $[VO_4]^{3-}$ to Eu^{3+} ions is more effective at higher Eu^{3+} concentrations because many Eu^{3+} ions are located near VO_4. As a result, the $[VO_4]^{3-}$ emission intensity is reduced at the lower Eu^{3+} concentrations.

The PL QE is also plotted against the Eu^{3+} concentration in Figure 6b. The maximum QE of 38.5% was obtained at x = 0.6. It was found that the concentration dependence is similar to the PL intensity. In Table 1, the QE values of undoped and Eu^{3+}-doped $CsK_2Gd[VO_4]_2$ are summarized together with the

Table 1. PL QE (%), PLE Band Peak (nm), and CIE of $CsK_2Gd_{1-x}Eu_x[VO_4]_2$ (x = 0−1.0) Compared to Some Reported Vanadates

phosphors	QE	λ_{ex}	CIE (x,y)	luminescence centers
x = 0	22.8	320	(0.316, 0.512)	VO_4^{3-}
x = 0.1	25.5	320	(0.315, 0.562)	Eu^{3+}, VO_4^{3-}
x = 0.2	24.7	320	(0.425, 0.458)	Eu^{3+}, VO_4^{3-}
x = 0.3	23.5	320	(0.431, 0.441)	Eu^{3+}, VO_4^{3-}
x = 0.4	24.7	320	(0.445, 0.431)	Eu^{3+}, VO_4^{3-}
x = 0.5	31.5	320	(0.450, 0.410)	Eu^{3+}, VO_4^{3-}
x = 0.6	38.5	320	(0.451, 0.423)	Eu^{3+}, VO_4^{3-}
x = 0.7	38.2	320	(0.441, 0.431)	Eu^{3+}, VO_4^{3-}
x = 0.8	34.1	320	(0.452, 0.421)	Eu^{3+}, VO_4^{3-}
x = 0.9	27.7	320	(0.435, 0.411)	Eu^{3+}, VO_4^{3-}
$Ca_5Mg_4(VO_4)_6$[37]	41.6	320	(0.382, 0.499)	VO_4^{3}
$Ca_5Zn_4(VO_4)_6$[37]	15.9	320	(0.425, 0.511)	VO_4^{3-}
$CsVO_3$[8]	87.0	350	(0.306, 0.418)	VO_4^{3-}
$Zn_3(VO_4)_2$[8]	52.0	350	(0.432, 0.478)	VO_4^{3-}
$Ba_2V_2O_7$[8]	25.0	350	(0.277, 0.389)	VO_4^{3-}
$Mg_3(VO_4)_2$[8]	6.0	350	(0.449, 0.475)	VO_4^{3-}
$Sr_3(VO_4)_2$[8]	3.7	350	(0.329, 0.415)	VO_4^{3-}
KVO_3[28]	4.0	350	(0.362, 0.453)	VO_4^{3-}
$Ca_2NaZn_2V_3O_{12}$[8]	11.4	365	(0.214, 0.338)	VO_4^{3-}
$Ca_2NaZn_2V_3O_{12}$:Eu^{3+}[28]	17.4	365	(0.291, 0.359)	Eu^{3+}, VO_4^{3-}

QEs of the other vanadates for comparison. The undoped $CsK_2Gd[VO_4]_2$ had a QE of 22.8%, which is much lower than the QEs of $Ca_5Mg_4(VO_4)_6$, $CsVO_3$, and $Zn_3(VO_4)_2$; however, it is comparable to the QE of $Ba_2V_2O_7$ and higher than the QEs of the other vanadates.

The PL spectra of $CsK_2Gd_{1-x}Eu_x[VO_4]_2$ (x = 0−1.0) excited at 365 nm are shown in Figure 7a. The 365 nm excitation refers to the excitation into $[VO_4]^{3-}$. Unlike Figure 6a of the excitation into Eu^{3+} ions located nearby VO_4 at 312 nm, the 530 nm host emission band shows a red-shift with the increasing Eu^{3+} concentration. The PLE band also shows a red-shift as shown in Figure 7b. This indicates the influence of the Eu^{3+} ions on the VO_4 host emission, which is understood as follows. Ronde et al.[38] have suggested that the energy of the $[VO_4]^{3-}$ charge−transfer transition depends on the V—O distance. The transition energies ΔE (t_1-2e) decrease with the increasing V—O distance. The XRD of Figure 1 indicates that the lattice expansion with the increasing Eu^{3+} concentration is because of the larger Eu^{3+} ion radius than Gd^{3+} ion radius as mentioned in section 3.1. In this way we understand the red-shift.

Figure 8 shows the decay curves measured by monitoring the 530 nm emission from the host and the 593 nm emission from the Eu^{3+} ions. Nonexponential decay curves are observed. They are fitted to a biexponential model as follows:[39]

$$y(t) = A_1 \exp(-t/\tau_1) + A_2 \exp(-t/\tau_2) + y_0 \quad (1)$$

where $y(t)$ represents the luminescence intensity at a time t after the cut off of the excitation light. A_1 and A_2 are pre-exponential factors associated with the lifetime components τ_1 and τ_2, respectively. The average lifetimes can be calculated by eq 2.

dx.doi.org/10.1021/ic500208h | Inorg. Chem. 2014, 53, 4161−4168

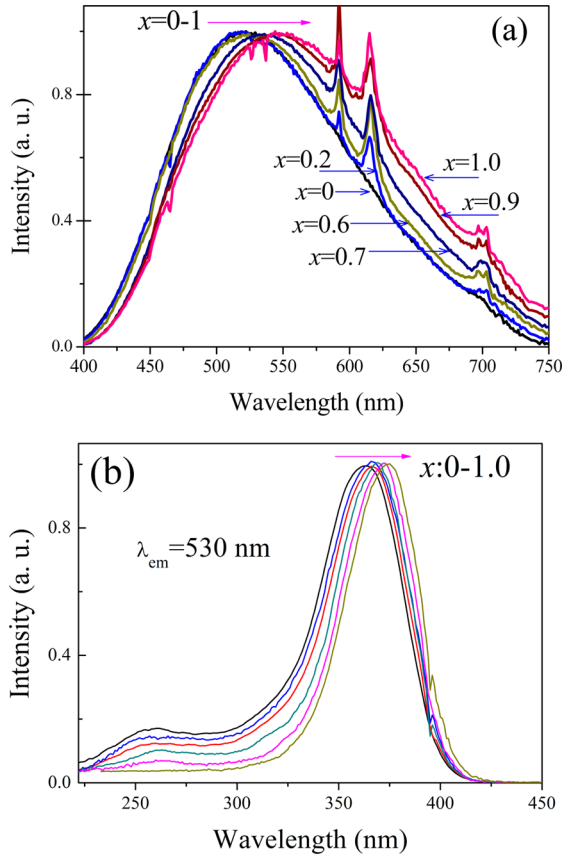

Figure 7. (a) Normalized PL spectra of $CsK_2Gd_{1-x}Eu_x[VO_4]_2$ (x = 0–1.0) excited at 365 nm. (b) Normalized PLE spectra of $CsK_2Gd_{1-x}Eu_x[VO_4]_2$ (x = 0–1.0).

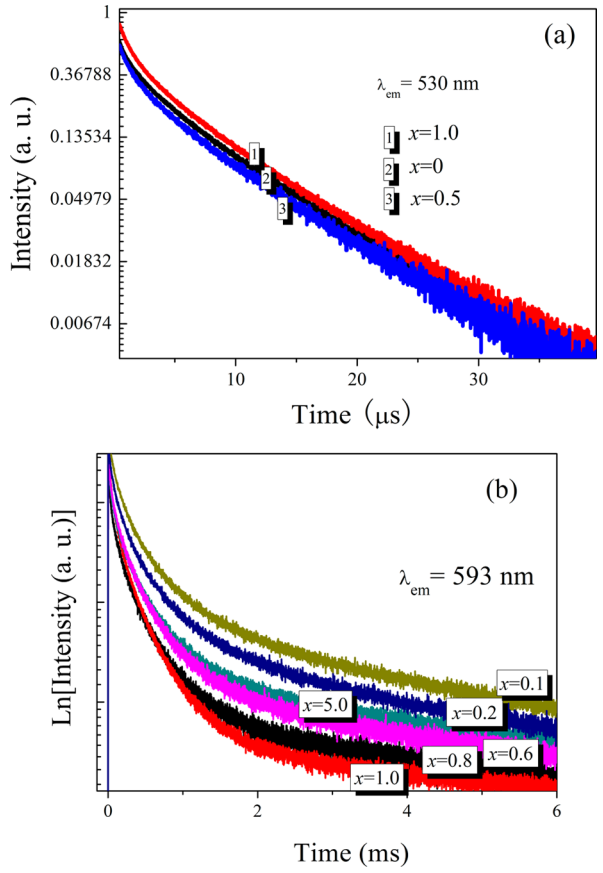

Figure 8. Decay curves of 530 nm (a) and 593 nm (b) in $CsK_2Gd_{1-x}Eu_x[VO_4]_2$ (x = 0–1.0) phosphors, under the excitation of 266 nm.

$$t_{average} = \frac{A_1\tau_1 + A_2\tau_2^{\,2}}{A_1\tau_1 + A_2\tau_2} \quad (2)$$

The average lifetimes of the 530 and 593 nm emissions, which were estimated at various concentrations, are summarized in Table 2.

The 530 nm emission took almost the same decay time between the undoped and doped samples. The average lifetime kept nearly the same value for the variations of the Eu^{3+} concentration. For example, the lifetimes of undoped samples of $CsK_2Gd[VO_4]_2$ and highly Eu^{3+}-doped $CsK_2Eu[VO_4]_2$ were 6.33 and 6.26 μs, respectively. The two values are close to each other. Such long lifetimes of this order confirm that the 530 nm emission is due to the original spin-forbidden transition and that the 530 nm emission arises from VO_4. The 593 nm emission due to Eu^{3+} takes a much longer decay time for all of the doped samples than did the 530 nm emission. This is reasonable because the emission is due to the parity-forbidden *f-f* transition in addition to the spin-forbidden transition.

Finally we discuss the inefficient energy transfer from VO_4 to Eu^{3+}, which allows both the VO_4 and Eu^{3+} emissions. The $[VO_4]^{3-} \rightarrow Eu^{3+}$ energy transfer (ET) occurs via either an exchange or superexchange mechanism, where the ET rate depends on the V—O—Eu bond angle.[40,41] In Eu^{3+}-doped materials with highly charged transition metal ion (M) complexes such as tungstates and molybdates, a 180° angle of M—O—Eu (i.e., linear coordination structure) maximizes the wave function overlap and enhances the ET efficiency.[8] As seen in Figure 2b, the V—O—Eu bond angle is about 160°, which reduces the wave function overlap and the exchange ET efficiency. Consequently, the emission from VO_4 in $CsK_2Gd_{1-x}Eu_x[VO_4]_2$ never disappears. Moreover, it is seen from Figure 2a that there are parallel chains formed by the cation-poyhedra in the $CsK_2Gd[VO_4]_2$ lattices. The octahedral $Gd(Eu)^{3+}$ ions are structurally separated from the VO_4 groups by two chains formed by $M(1)O_{10}$ (0.67K + 0.33Cs) and $M(2)O_{12}$ (0.67K + 0.33Cs) polyhedra cations. This also contributes to the inefficient ET of $[VO_4]^{3-} \rightarrow Eu^{3+}$.

Table 2. Average Lifetimes of the 530 nm VO_4 Emission (μs) and the 593 nm Eu^{3+} Emission (ms) in $CsK_2Gd_{1-x}Eu_x[VO_4]_2$ (x = 0–1.0)

x	530 nm (μs)	593 nm (ms)
0	6.33	
0.1	6.37	0.61
0.2	6.44	0.52
0.3	6.5	0.63
0.4	6.51	0.68
0.5	6.21	0.72
0.6	6.08	0.81
0.7	6.59	1.02
0.8	6.02	2.41
0.9	6.33	2.15
1.0	6.26	2.05

dx.doi.org/10.1021/ic500208h | Inorg. Chem. 2014, 53, 4161–4168

4. CONCLUSIONS

Undoped and Eu^{3+}-doped glaserite-type orthovanadates $CsK_2Gd_{1-x}Eu_x[VO_4]_2$ with various Eu^{3+} concentrations of x = 0, 0.1, 0.2, 0.3, 0.4, 0.5, 0.6, 0.7, 0.8, 0.9, and 1.0 were synthesized via the solid-state reaction. The undoped $CsK_2Gd(VO_4)$ shows a broad emission band with a maximum at 530 nm due to the CT transitions in VO_4. The doped $CsK_2Gd_{1-x}Eu_x[VO_4]_2$ (x = 0.1−0.9) showed the broad emission band with a maximum at 530 nm due to the VO_4 host and sharp emission lines due to the transitions from the excited $^5D_0$ state to the Stark components of ^7F_J (J = 0−4) levels in Eu^{3+}. Unlike the previously reported results for Eu^{3+}-doped vanadates, Eu^{3+}-doped orthovanadates showed nonquenching of the host emission even when in the Eu^{3+}-condensed host of $CsK_2Eu(VO_4)$; that is, x = 1.0 in $CsK_2Gd_{1-x}Eu_x[VO_4]_2$. This supports that the 530 nm emission has been attributed to $[VO_4]^{3-}$, independent of Gd^{3+}. The intensity of the host emission from $[VO_4]^{3-}$ increases with increases in the Eu^{3+} concentration from x = 0 to x = 0.6 and decreases with increases from x = 0.6 to x = 1.0. Two broad PLE bands with maxima at 330 and 312 nm are observed for the Eu^{3+} emission, which are not observed in the undoped sample. Observation of the nondisappearance of the host emission under UV excitation indicates inefficient ET from host $[VO_4]^{3-}$ to Eu^{3+}. This is understood by the suppression of the ET by the V^{5+}—O^{2-}—Eu^{3+} bond angle when it is deviated from 180° and the separation of the Eu^{3+} ions at Gd^{3+} sites from the VO_4 by two kinds of chains formed by $M(1)O_{10}$ (0.67K + 0.33Cs) and $M(2)O_{12}$ (0.67K + 0.33Cs) polyhedra cations. This phosphor shows tunable color from green to yellow and red by changing the excitation wavelength. The white color can be realized by combining the broad emission band due to $[VO_4]^{3-}$ with the intense sharp lines due to Eu^{3+}, in a single phase Eu^{3+}-doped $CsK_2Gd[VO_4]_2$ under excitation with UV light. Taking into account that the maximum photoluminescence QE of 38.5% was obtained in $CsK_2Gd_{1-x}Eu_x[VO_4]_2$ (x = 0.6) at room temperature and that photoluminescence with a white color is obtained, this material is suggested to be useful for lighting under the excitation of UV or near-UV light.

■ AUTHOR INFORMATION

Corresponding Author

*E-mail: hjseo@pknu.ac.kr. Phone: +82-51-629 5568. Fax:+82-51-6295549.

Notes

The authors declare no competing financial interest.

■ ACKNOWLEDGMENTS

This work was supported by the Basic Science Research Program through the National Research Foundation of Korea (NRF) funded by the Ministry of Science, ICT & Future Planning (NRF-2013R1A1A2009154) and by the Priority Academic Program Development of Jiangsu Higher Education Institutions (PAPD), China.

■ REFERENCES

(1) Nakajima, T.; Isobe, M.; Tsuchiya, T.; Ueda, Y.; Kumagai, T. *J. Lumin.* **2009**, *129*, 1598−1601.
(2) Dhobale, A. R.; Mohapatra, M.; Natarajan, V.; Godbol, S. V. *J. Lumin.* **2012**, *132*, 293−298.
(3) Gundiah, G.; Shimomura, Y.; Kijima, N.; Cheetham, A. K. *Chem. Phys. Lett.* **2008**, *455*, 279−283.
(4) Lin, H. Y.; Chu, S. Y. *J. Am. Ceram. Soc.* **2012**, *95*, 3538−3546.
(5) Benmokhtar, S.; Jazouli, A. E.; Chaminade, J. P.; Gravereau, P.; Guillen, F.; Waal, D. D. *J. Solid State Chem.* **2004**, *177*, 4175−4182.
(6) Chen, L.; Chen, K. J.; Hud, S. F.; Liu, R. S. *J. Mater. Chem.* **2011**, *21*, 3677−3685.
(7) Nishida, T.; Ban, T.; Kobayashi, N. *Appl. Phys. Lett.* **2003**, *82*, 3817−3819.
(8) Nakajima, T.; Isobe, M.; Tsuchiya, T.; Ueda, Y.; Manabe, T. *J. Phys. Chem. C* **2010**, *114*, 5160−5167.
(9) Setlur, A. A.; Comanzo, H. A.; Srivatava, A. M.; Beers, W. W. *J. Electrochem. Soc.* **2005**, *152*, H205−H208.
(10) Liu, L.; Xie, R. J.; Hirosaki, N.; Li, Y.; Takeda, T.; Zhang, C. N.; Li, J.; Sun, X. *J. Am. Ceram. Soc.* **2010**, *93*, 4081−4086.
(11) Park, K. C.; Mho, S. I. *J. Lumin.* **2007**, *122*−*123*, 95−98.
(12) Kharsika, V. F.; Komissarova, L. N.; Kirichenko, A. N.; Murav'ev, E. N.; Orlovskii, V. P.; Chernyaev, A. P. *Inorg. Mater.* **2001**, *37*, 831−835.
(13) Higuchi, T.; Hotta, Y.; Hikita, Y.; Maruyama, S.; Hayamizu, Y.; Akiyama, H.; Wadati, H.; Hawthorn, D. G.; Regier, T. Z.; Blyth, R. I. R.; Sawatzky, G. A.; Hwang, H. Y. *Appl. Phys. Lett.* **2011**, *98*, 071902.
(14) Wang, W.; Cheng, Z.; Yang, P.; Hou, Z.; Li, C.; Li, G.; Dai, Y.; Lin, J. *Adv. Funct. Mater.* **2011**, *21*, 456−463.
(15) Toma, S. Z.; Mikus, F. F.; Mathers, J. E. *J. Electrochem. Soc.* **1967**, *114*, 953−955.
(16) Yamamoto, H.; Seki, S.; Jeser, J. P.; Ishiba, T. *J. Electrochem. Soc.* **1980**, *127*, 694−701.
(17) Kimani, M. M.; Kolis, J. W. *J. Lumin.* **2014**, *145*, 492−497.
(18) Kimani, M. M.; Thompson, L.; Snider, W.; McMillen, C. D.; Kolis, J. W. *Inorg. Chem.* **2012**, *51*, 13271−13280.
(19) Salmon, R.; Parent, C.; Flem, G. L.; Vlasse, M. *Acta Crystallogr., Sect. B* **1976**, *32*, 2799−2802.
(20) Mel'nikov, P. P.; Komissarova, L. N.; Efremov, V. A.; Carillo Eredero, H. D. *Inorg. Mater.* **1987**, *23*, 1395.
(21) Boukhris, A.; Hidouri, M.; Glorieux, B.; Ben Amara, M. *Mater. Chem. Phys.* **2012**, *137*, 26−33.
(22) Sayer, M. *Phys. Status Solidi A* **1970**, *1*, 269−277.
(23) Schiff, L. I. *Quantum Mechanics*; McGraw-Hill Book Co.: New York, 1955; Section 38.
(24) Ronde, H.; Blasse, G. *J. Inorg. Nucl. Chem.* **1978**, *40*, 215−219.
(25) Yu, M.; Lin, J.; Wang, Z.; Fu, J.; Wang, S.; Zhang, H. J.; Han, Y. C. *Chem. Mater.* **2002**, *14*, 2224−2231.
(26) Xu, Z.; Kang, X.; Li, C.; Hou, Z.; Zhang, C.; Yang, D.; Li, G.; Lin, J. *Inorg. Chem.* **2010**, *49*, 6706−6715.
(27) Wu, C. C.; Chen, K. B.; Lee, C. S.; Chen, T. M.; Cheng, B. M. *Chem. Mater.* **2007**, *19*, 3278−3285.
(28) Chen, X.; Xia, Z. G.; Yi, M.; Wu, X. C.; Xin, H. J. *Phys. Chem. Solids* **2013**, *74*, 1439−1443.
(29) Tallant, D. R.; Seager, C. H.; Simpson, R. L. J. *Appl. Phys.* **2002**, *91*, 4053−4064.
(30) Lu, Q.; Wang, Z.; Wang, P.; Li, J. *Nanoscale Res. Lett.* **2010**, *5*, 761−768.
(31) Tian, Y.; Jiao, X.; Zhang, J.; Sui, N.; Chen, D.; Hong, G. J. *J. Nanopart. Res.* **2010**, *12*, 161−168.
(32) Chen, H.; Lian, R.; Yin, M.; Lou, L.; Zhang, W.; Xia, S.; Krupa, J. C. J. *Phys. Condens. Matter* **2001**, *13*, 1151−1158.
(33) Collins, J.; Geen, M.; Bettinelli, M.; Di Bartolo, B. J. *J. Lumin.* **2012**, *132*, 2626−2633.
(34) Dai, S.; Yu, C.; Zhou, G.; Zhang, J.; Wang, G.; Hu, L. J. *J. Lumin.* **2006**, *117*, 39−45.
(35) Jaba, N.; Ben Mansour, H.; Kanoun, A.; Brenier, A.; Champagnon, B. J. *J. Lumin.* **2009**, *129*, 270−276.
(36) Sontakke, A. D.; Annapurna, K. *Mater. Chem. Phys.* **2013**, *137*, 916−921.
(37) Huang, Y. L.; Yu, Y. M.; Tsuboi, T.; Seo, H. J. *Opt. Express* **2012**, *20*, 4360−4368.
(38) Ronde, H.; Snijder, J. G. *Chem. Phys. Lett.* **1977**, *50*, 282−283.

(39) Mihokova, E.; Nikl, M.; Mares, J. A.; Beitlerova, A.; Vedda, A.; Nejezchleb, K.; Blazek, K.; Ambrosio, C. D. *J. Lumin.* **2007**, *126*, 77−80.
(40) Blasse, G.; Bril, A. *J. Electrochem. Soc.* **1967**, *114*, 250−252.
(41) Hsu, C.; Powell, R. C. *J. Lumin.* **1975**, *10*, 273−293.